11-20-2017

Hydrologic exchange and chemical weathering in a proglacial watershed near Kangerlussuaq, west Greenland

Kelly M. Deuerling

Jonathan B. Martin

Ellen E. Martin

Cecilia A. Scribner

Hydrologic exchange and chemical weathering in a proglacial watershed near Kangerlussuaq, west Greenland

Kelly M. Deuerling, Jonathan B. Martin, Ellen E. Martin, Cecilia A. Scribner
Department of Geological Sciences, University of Florida, Gainesville, FL 32611, USA
https://doi.org/10.1016/j.jhydrol.2017.11.0020022-1694/

ABSTRACT

The exchange of proglacial river water with active layer pore water could alter water chemical compositions in glacial outwash plains and oceanic solute fluxes. To evaluate effects of this exchange, we sampled Watson River and adjacent pore water during the 2013 melt season at two sandurs in western Greenland; one in Sandflugtdalen and the other near the confluence with Søndre Strømfjord. We measured temperature, specific conductivity, and head gradients between the river and bank over a week-long period at Sandflugtdalen, as well as sediment hydraulic conductivity and chemical compositions of waters from both sites. Specific conductivity of pore water is four to ten times greater than river water as solutes are concentrated from weathering reactions, cryoconcentration, and evaporation. Pore water compositions are predominantly altered by carbonate dissolution and sulfide mineral oxidation. High concentrations of HCO_3 and SO_4 result from solute recycling and dissolution of secondary Ca-Mg carbonate/sulfate salts initially formed by near-surface evaporation in the summer and at depth by freeze-in of the active layer and cryoconcentration in the winter. High hydraulic conductivity (10^{-5} to 10^{-4} m/s) and diurnal fluctuations of river stage during our study caused exchange of river and pore water immediately adjacent to the river channel, with a net loss of river water to the bank. Pore water >6 m from the river continuously flowed away from the river. Approximately 1–8% of the river discharge through the Sandflugtdalen was lost to the river bank during our 6.75 day study based on calculations using Darcy's Law. Although not sampled, some of this water should discharge to the river during low river stage early and late in the melt season. Elevated pore water solute concentrations in sandurs and water exchange at

diurnal and seasonal frequency should impact fluxes of solutes to the ocean, although under- standing the magnitude of this effect will require long-term evaluation throughout the melt season.

Keywords: Hydrologic exchange flows, Bank storage, Glacial weathering, Chemical weathering, Proglacial, Greenland

1. Introduction

High physical weathering rates in glacial terrains produce freshly eroded, fine-grained, reactive sediments that are commonly trapped in large outwash plains (sandurs) along glacial rivers. The reactive characteristics of the sediment result in chemical weathering rates in proglacial watersheds that are similar to those of temperate watersheds with similar specific discharge despite low temperatures (e.g., Anderson et al., 1997). Chemical weathering reactions are dominated by preferential weathering of trace reactive mineral phases (carbonate, biotite) and oxidation of sulfide minerals in subglacial and proglacial watersheds of alpine glaciers (e.g., Anderson, 2007; Tranter, 2003). Rates and magnitudes of weathering depend on which acid causes weathering and which minerals weather, and are important for nutrient and radiogenic isotope fluxes to the ocean (Crocket et al., 2012; Hawkings et al., 2016, 2015; Kurzweil et al., 2010) as well as exchange with atmospheric CO_2 (Berner et al., 1983; Martin, 2017; Spence and Telmer, 2005). Much of the weathering in proglacial rivers may occur in sandurs because they trap comminuted sediment and thereby extend the sediment residence times; however, the impact of weathering in sandurs depends on pore water residence times and thus the rate and direction of exchange between pore water and river water.

This exchange between sandur pore water and proglacial rivers depends on sediment permeability and head gradients between the river and its bank. It also may occur during flooding of the top of the sandur sediments and from percolation of precipitation (snow and/or rain into the exposed sandur). In this paper we refer to this exchange as ‘‘hydrologic exchange flow”, which describes all lateral and vertical exchange of river and subsurface waters rather than the more commonly used, but

more restricted term, hyperheic exchange (Harvey and Gooseff, 2015). Head gradients of proglacial streams should vary at diurnal and seasonal timescales as their flow varies with alternating freeze and thaw (Graly et al., 2017; Koch et al., 2011; Malard et al., 1999). Permeability may also vary in permafrost-affected areas during freeze in of groundwater and restrict hydrologic exchange flow. However, streams in the Arctic tundra of Alaska were found to contribute bioreactive solutes at rates similar to temperate ecosystems (Edwardson et al., 2003). Altered pore water compositions, and their contributions to river compositions, should be enhanced by low water-rock ratios and long residence times compared to water in the river channel (Nezat et al., 2001) that produce steep gradients of biogeochemically reactive solutes (Boulton et al., 1998). For example, the proglacial discharge from Finsterwalderbreen, Svalbard, has elevated Ca, Mg, SO_4, and HCO_3 concentrations from sulfide oxidation and carbonate and gypsum dissolution in the river bank, which enhance in-stream solute concentrations by 30–50% (Cooper et al., 2002; Wadham et al., 2001). Delivery of these solutes from pore waters to the streams depends on flow conditions and the extent of subsurface exchange, which varies over diurnal to seasonal timescales during the ablation season (Koch et al., 2011; Malard et al., 1999).

To assess the potential contributions from hydrologic exchange flow to a proglacial river draining a continental ice sheet, we evaluate chemical alteration in pore waters and hydrologic exchange between proglacial surface and pore waters at two locations along the Watson River near Kangerlussuaq, west Greenland. We also calculate temporary bank storage (proximal exchange) immediately adjacent to the river channel due to diurnal river stage fluctuations. We use these observations to speculate on distal exchange caused by seasonal changes in river stage (e.g., Gooseff et al., 2003). Our data include hydrologic parameters, major ion, and minor element hydrochemistry that provide an assessment of weathering reactions and how proglacial hydrologic exchange flows may affect river water chemical composition and potential oceanic solute fluxes. These data should be considered a reconnaissance study serving to expand our knowledge of hydrologic exchange flows in proglacial watersheds draining ice sheets. To our knowledge, this work represents the first study of hydrologic exchange flows and pore water chemistry

conducted in a proglacial watershed draining the Greenland Ice Sheet, an actively retreating continental ice sheet. Our results could be important for under- standing mechanisms for ocean and atmospheric fluxes during retreat of the northern hemisphere ice sheets since the last glacial maximum, and for making predications of changes in fluxes as glaciers continue to retreat in a warming world.

2. Methods

2.1. *Site description*

The Watson River flows ~40 km from the convergence of Isunnguata Sermia and Russell Glacier at the western margin of the Greenland Ice Sheet into Søndre Strømfjord (Fig. 1A), draining a proglacial area of ~600 km^2. Average summer discharge to Søndre Strømfjord was 117 m^3/s between 2007 and 2010 (Hasholt et al., 2013), correlating with increased ice melt and evolution of an efficient subglacial drainage system (Bartholomew et al., 2010; Chandler et al., 2013). We investigated two portions of the out- wash plain: Sandflugtdalen (67.06°N, 50.39°W) and a smaller san- dur across the Watson River from the Kangerlussuaq International Science Support (KISS) facility (67.00°N, 50.68°W), hereafter referred to as WR6 and WRK, respectively. Sampling locations at WR6 were located near the middle of the valley, while the sampled sandur at WRK abuts a hill. Near the river bank, glaciofluvial fine to coarse sands with intermittent gravel lenses predominate and give way to eolian sands with increasing vegetation and peat content with distance from the channel (Willemse et al., 2003). The down- stream site, WRK, consists of finer, better-sorted sands than WR6 within the depths sampled. The sampling regions in this study have longitudinal gradients of ~1.4 m/km at Sandflugtdalen (WR6), while transverse gradients are ~100 m/km (Howat et al., 2014). These gradients suggest lateral hydrologic exchange flows are likely larger than longitudinal hydrologic exchange flows and therefore we focus this study on lateral exchange.

Long-term (1958–1999) mean annual air temperature is -5.7°C in the Kangerlussuaq region. Mean annual precipitation is ~150 mm (Cappelen et al., 2001), while ~300 mm of evapotranspiration produces a negative water balance (Hasholt and Sogaard, 1978). Continuous permafrost has a seasonal active layer

thickness of up to 1.7 m on non-vegetated portions of the proglacial outwash area (Dijkmans and Tornqvist, 1991; van Tatenhove and Olesen, 1994).

Local bedrock consists of metamorphosed Archean gneisses of the Nagssugtoqidian mobile belt (NMB) (Escher and Watt, 1976). Major mineralogy includes quartz, potassium feldspars, and plagioclase along with minor amounts of biotite, muscovite, sphene, garnet, epidote, magnetite, amphibole, apatite, zircon, pyrite, chlorite, and calcite (Hindshaw et al., 2014; Mowatt and Naidu, 1994; Souchez et al., 1990; Yde et al., 2010). Trace calcite (average = 0.6 g/kg $CaCO_3$, n = 2) is also present in bedload sediments from the Watson River based on coulometric titration, consistent with carbonate concentrations in felsic rocks collected near Nuuk, Greenland (White et al., 2005). Primary carbonate rocks do not occur in the field region, thus any calcite present must be disseminated in the bedrock as a minor mineral phase (Killawee et al., 1998; White et al., 2005).

2.2. *Field methods*

2.2.1. *Water chemistry*

Pore water samples were collected from WR6 (14–15 July) and WRK (16 July) during the 2013 melt season (Fig. 1A); Watson River water samples were collected at both sites on 8 July. Pore water samples were collected using an AMS vapor probe (Charette and Allen, 2006) at discrete depths 20–96 cm below the water table (cmbwt). The vapor probe was installed in river bank sediments in a transect perpendicular to one of the larger braids in the river channel (Fig. 1B). During sampling, the channel remained straight and stable, although it widened with increased discharge during our sampling period. Both pore and river water were pumped into an overflow cup using a peristaltic pump fitted with tygon tubing. Temperature, pH, specific conductivity (SpC) corrected to 25 °C, and dissolved oxygen (DO) were measured with a YSI ProPlus handheld unit with the sonde installed in the overflow cup. Once readings stabilized, sample water was filtered through a 0.45 µm trace metal grade canister filter into labeled bottles and preserved as required for each solute. Cation and dissolved metal samples were collected in acid-washed 20 mL HDPE bottles and preserved with Optima HNO_3 to pH < 2. Dissolved inorganic carbon (DIC) samples were collected in 20 mL

glass vials and preserved with a saturated solution of mercuric chloride. Anion and silica samples were collected in DI-washed 20 mL HDPE bottles with no preservative. Stable isotope samples were collected in 2 mL borosilicate glass vials with no preservative. All bottles were triple rinsed with filtered site water before collecting the sample for analysis. Water isotope and DIC samples were collected to minimize headspace in vials. Silica was analyzed within thirty days of collection at the laboratory facilities at KISS. All other samples were stored at KISS in 4 °C refrigerators. Samples were shipped chilled to the University of Florida and stored at 4 °C until analysis.

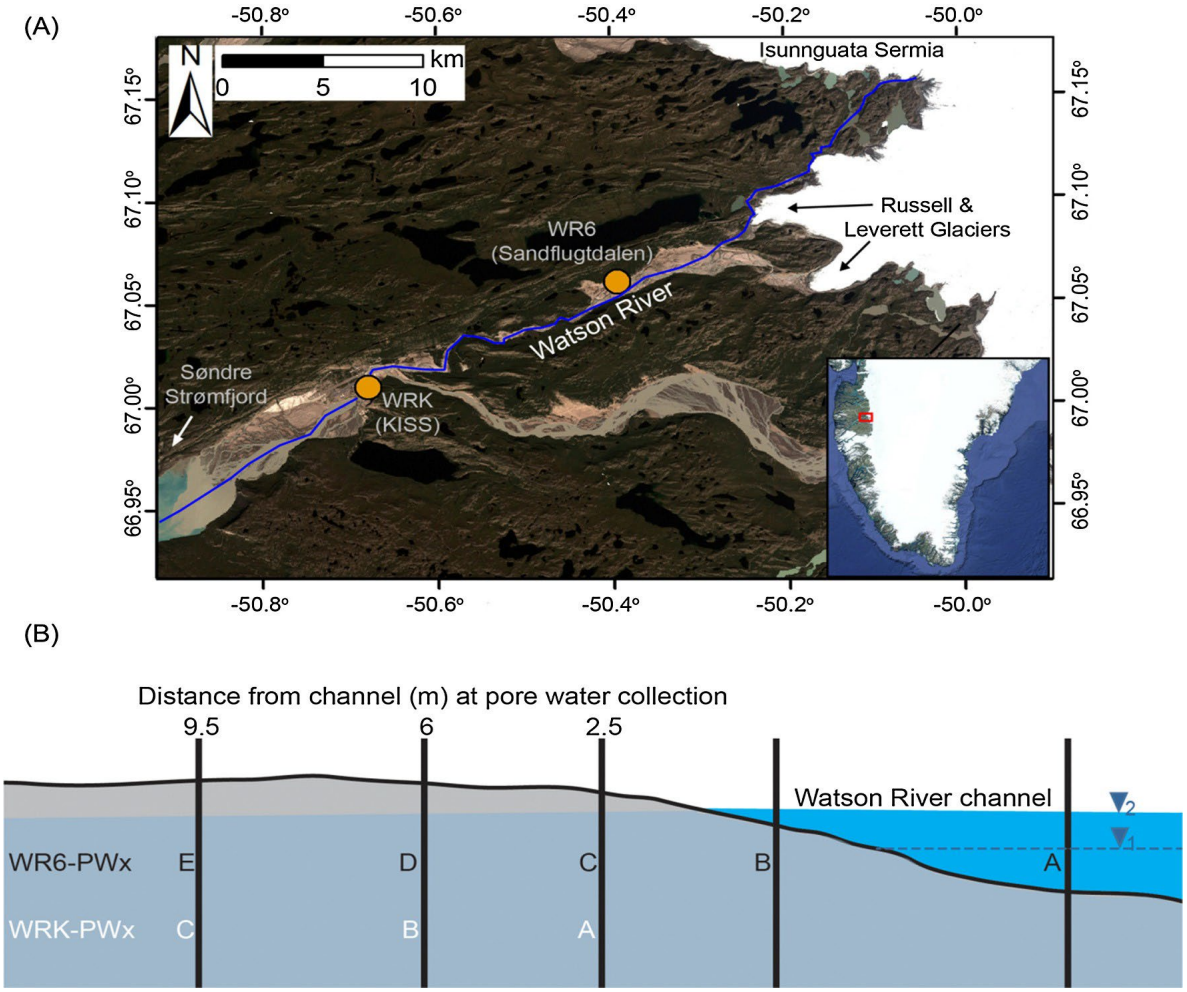

Fig. 1. A) Landsat image of Kangerlussuaq region of western Greenland. Watson River locations and pore water transect locations are highlighted for reference. Arrow indicates direction of Søndre Strømfjord. Inset map of southern Greenland with sampling region highlighted in red. Blue line highlights the approximate route of the Watson River. B) Schematic of pore water and CTD deployment locations at WR6 and WRK. Black bars indicate placement of piezometer or vapor probe at each site relative to river channel. $_{-1}$ indicates river level when piezometers were installed; $_{-2}$ indicates river level when piezometers were removed.

2.2.2. *Hydraulic measurements*

Hydraulic measurements were made at WR6, using four piezometers measuring 72 cm with a 23.5 cm screened interval and 3.2 cm internal diameter that were installed several meters upstream of the pore water sampling. The separation limited artifacts that may have results from pumping of pore water. The piezometers were spaced at 2.5, 6.0, 9.5, and 13.5 m from the edge of the channel and a fifth piezometer was installed in the river channel (Fig. 1B). Piezometers were driven with a sledge hammer into pits dug into the sediment to ensure installation below the water table. These piezometers were instrumented with conductivity-temperature-depth (CTD) sondes that recorded SpC, temperature and pressure once per minute for one week (7–14 July 2013). Head differences (dh) between river and pore water were calculated by subtracting the atmospheric pressure-corrected (Rennermalm et al., 2014) pressures logged by the river CTD from the CTDs installed in the bank sediment based on a datum of water level dug in a channel from the river to the farthest piezometer at the end of the experiment. The distance between the piezometers (dL) was measured to calculate the head gradient (dh/dL) between the CTDs in the river and the bank sediments.

Saturated zone hydraulic conductivity, K_{sat}, was determined ~20 m upstream of hydraulic conductivity calculation sites using a falling head slug test (Bouwer and Rice, 1976). These tests were conducted with piezometers similar to those in the monitoring transect. CTDs recording at 1 Hz were mounted in the piezometers just below the water table and allowed to equilibrate. River water was poured into the piezometer until they overflowed for at least five seconds, then the system was allowed to return to baseline. This process was repeated four times at each site and three sites were measured at both locations. Hydraulic conductivity was calculated assuming an unconfined aquifer with:

$$K_{sat} = \frac{r_c^2 \ln(R_e/r_w)}{2L} \frac{1}{t} ln\left(\frac{h_0}{h_t}\right)$$

(Bouwer and Rice, 1976), where r_c and r_w are the internal and external radii of the piezometer, R_e is the effective radial distance over which the increase in head is dissipated, L is the length of the screen in the piezometer, h_0 is the maximum head displacement at time t = 0, and h_t is the head displacement at time t. Because R_e is

not known, we estimate the R_e/r_w ratio based on the method of Bouwer (1989) for partially penetrating wells:

$$ln\frac{R_e}{r_w} = \left[\frac{1.1}{ln(L_w/r_w)} + \frac{A + B\,ln[(L_b - L_w)/r_w]}{L/r_w}\right]$$

where L_w is the distance from the bottom of the well to the water table, L_b is the distance from the water table to the bottom of the aquifer, here assumed to be the top of the permafrost, and A and B are dimensionless constants based on L/r_w. The head gradients and hydraulic conductivity were used to estimate fluxes of river water into and out of the bank sediments based on Darcy's Law:

$$Q = -AK\frac{dh}{dL}$$

where Q (L^3/t) is the recharge into the sediment or discharge to the river depending on the sign of the head gradient and A is a unit area of the bed of the river. We lack head gradient values for the WRK site and thus estimate recharge to the sediment and discharge to the river (Eq. (3)) only at WR6.

2.3. *Laboratory methods*

Silica was analyzed using the low-range Heteropoly Blue method (0–1.6 mg/L SiO_2) on a Hach DR/890 portable colorimeter. Samples with measured SiO_2 concentrations >1.6 mg/L were diluted and reanalyzed within the range of the method. Duplicate samples and repeated standard measurements agreed within 10%.

Concentrations of DIC were measured on CO_2 extracted by acidification using an AutoMate Prep Device coupled to a UIC (Coulometrics) 5011 carbon coulometer. Repeated analyses of a 24.0 µg C/g standard agreed within 1%. Oxygen and hydrogen isotopes were measured on a Picarro L2120-I Isotopic Liquid Water & Certified Continuous Water Vapor Analyzer fit with a Picarro A0211 High Precision Vaporizer and a CTC HTS PAL autosampler. Isotope results are reported in delta notation relative to Vienna Standard Mean Ocean Water. Repeated analyses of an in-house standard had a relative standard deviation of 4% for $\delta^{18}O$ and 8% for δD.

Major ion concentrations (Na, K, Mg, Ca, Cl, and SO_4) were measured on a Dionex ICS-1600 (cations) and ICS-2100 (anions) ion chromatograph using custom

multi-element standards. Repeat measurement of a diluted Dionex stock multi-element standard and sample duplicates reproduced within 5%. Minor elemental concentrations (Al, Mn, Fe, Sr, Ba, Pb) were analyzed on a Thermo-Finnigan Element 2 ICP-MS. Samples were diluted with 5% HNO_3 spiked with 8 ppb Re and Rh to a dilution factor of two, then analyzed using custom multi-element standards. Canadian river standard SLRS4 was measured every 5–6 samples to check for instrumental drift and assess long-term reproducibility. The relative standard deviation for all elements based on SLRS4 was <8%. Major and minor element concentrations, temperature, pH, DO, and DIC concentrations were used to calculate solute speciation and mineral saturation states in PHREEQC (Parkhurst and Appelo, 1999). Average charge balance errors calculated using speciated HCO_3 and CO_3 from PHREEQC model were 4% for pore waters and 15% for Watson River water. Greater average charge balance errors in Watson River water are unsurprising given the low ionic strength of the water, which approached the detection limit of the techniques.

2.4. *Weathering reactions*

We analyze our data in part through comparisons with water compositions expected from the stoichiometry of various chemical reactions. Reactions of interest include dissolution of carbonate minerals through the hydration of CO_2 to carbonic acid or through oxidation of Fe-sulfide minerals to sulfuric acid including carbon- ate weathering by carbonic acid:

$$Ca_XMg_{(1-X)}CO_3 + H_2O + CO_2 \leftrightarrow XCa^{2+} + (1-X)Mg^{2+} + 2HCO_3^-$$

sulfide mineral oxidation:

$$4FeS_2 + 15O_2 + 14H_2O \leftrightarrow 8SO_4^{2-} + 16H^+ + 3Fe(OH)_3$$

sulfide mineral oxidation coupled to carbonate dissolution:

$$4FeS_2 + 16Ca_XMg_{(1-X)}CO_3 + 15O_2 + 14H_2O \leftrightarrow 16XCa^{2+} + 16(1-X)Mg^{2+} + 16HCO_3^- + 8SO_4^{2-} + 4Fe(OH)_3$$

And Ca-Mg silicate weathering by carbonic acid:

$$Ca_XMg_{(1-X)}SiO_3 + H_2O + CO_2 \leftrightarrow XCa^{2+} + (1-X)Mg^{2+} + 2HCO_3^- + SiO_2$$

If carbonate minerals dissolve according to reaction 4 utilizing only carbonic acid, bicarbonate concentrations increase without altering SO_4 concentrations. However, when sulfuric acid produced from sulfide mineral oxidation (reaction 5) dissolves carbonate minerals (reaction 6), the HCO_3:SO_4 ratio should equal 2.

Water in proglacial landscapes may be concentrated through freezing and evaporation on seasonal timescales leading to the secondary precipitation of evaporite minerals such as gypsum. These salts are quickly re-dissolved by low concentration melt waters during the melt season according to the reaction:

$$CaSO_4 2H_2O \leftrightarrow Ca^{2+} + SO_4^{2-} + 2H_2O$$

We calculate Ca + Mg derived from reactions other than carbon- ate or silicate mineral weathering, $(Ca + Mg)_{ex}$, in our water samples to quantify the influence of seasonal salts on Watson River surface and pore waters according to:

$$(Ca + Mg)_{ex} = [Ca + Mg] - 0.5^*[HCO_3]$$

where [Ca + Mg] and [HCO_3] are micromolar concentrations.

3. Results

3.1. *River water versus pore water composition*

Specific conductivity, pH and temperature show systematic variations with depth in the sediment and distance from the river (Fig. 2). Specific conductivity is greater in pore water than in river water and the pore water SpC increases with distance from the river (Fig. 2A). At sites near the river, the greatest SpC occurs at the greatest depth sampled (~90 cmbwt) but at sites farthest from the river the greatest SpC occurs at the shallowest depth and decreases with depth. Most pore water has greater SpC at WRK than WR6. Most pore water pH is greater than river water pH, with the exception of the distal site at WRK (Fig. 2). The trends in pH with depth and with distance from river are opposite to those seen in SpC. The lowest pH values occur at in the deepest sample at any one site, and decrease away from the river at both WR6 and WRK. Temperature in the pore water is generally greater than

the river water near the surface (20 cmbwt) and decreases with depth and distance from the river (Fig. 2C).

The distribution of major element concentrations follow systematic patterns between river water and pore water at WR6 and WRK (Fig. 3). Anions in river water are dominated by HCO_3 + CO_3, while pore waters have a greater relative abundance of SO_4 (Fig. 3A). WRK is enriched in SO_4 relative to WR6, which has relative concentrations intermediate between WRK and river values. Relative SO_4 concentrations of pore water increase with distance from river. For cations, the Watson River samples have greater relative concentrations of Si and Na + K compared to pore waters, which are enriched in Ca + Mg (Fig. 3B).

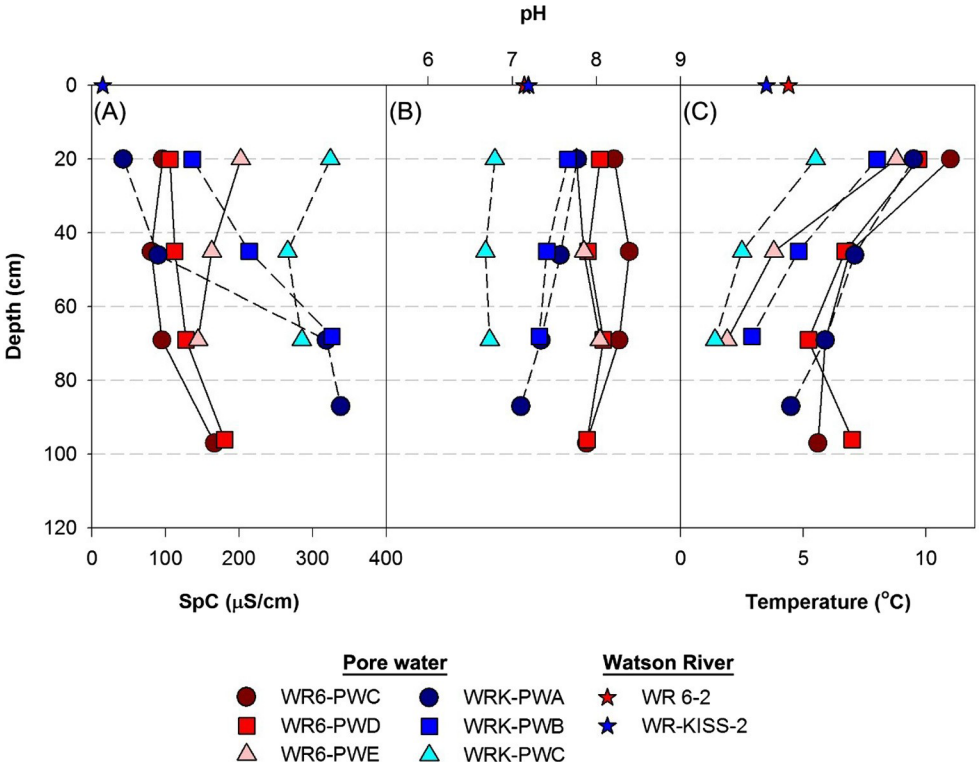

Fig. 2. Depth profiles of A) SpC, B) pH, and C) temperature at WR6 (filled symbols) and WRK (open symbols). Blue and red stars at surface (depth = 0 cm) represent the Watson River composition adjacent to pore water transects. (For interpretation of the references to colour in this figure legend, the reader is referred to the web version of this article.)

Relationships between pH, SO_4 and HCO_3 provide information about acid-base reactions in the pore water (Fig. 4). A significant inverse correlation exists between pH and SO_4 (r^2 = 0.70, p <.0001) in all pore waters and both differ from river water values, which have low SO_4 concentrations and approximately neutral pH (Fig.

4A). Sulfate concentrations increase and pH values decrease with distance from the river channel and depth in the sediment near the river channel. The highest SO_4 concentrations and lowest pH values occur in shallow pore water far from the river (Fig. 4A; Appendix 1). River water and most WR6 pore water have excess HCO_3 relative to the expected 2:1 molar ratio (reaction 5), with the exception of samples from 20 and 45 cmbwt at the distal location (WR6-PWE) (Fig. 4B). In contrast, WRK pore water sites have excess SO_4 except at the 20 cmbwt depth at the proximal site.

Mineral weathering can be identified based on relationships between Ca, Ca + Mg, Sr, and SO_4 (Fig. 5). A good correlation exists between Sr and Ca at WR6 (r^2 = 0.95, $p < .0001$) and WRK (r^2 = 0.97, $p < .0001$) with slopes of 0.78 (IM/nM) and 0.69 (IM/nM), respectively (Fig. 5A). Slopes of the regression indicate average Ca:Sr ratios are lower in WRK compared to WR6 pore waters, particularly far from the river. River water has Ca:Sr ratios of 0.99 (WR6) and 0.95 (WRK), near the intersection of compositions expected by weathering of carbonate and silicate mineral end members. Watson River water has Ca + Mg:HCO_3 ratios consistent with both carbonate and silicate weathering (Fig. 5B), but pore water Ca + Mg concentrations are greater relative to HCO_3 concentration than expected from carbonate and silicate weathering. The $(Ca + Mg)_{ex}$ values (e.g., values corrected for a source from carbon- ate dissolution, eq. 8) correlate significantly with SO_4 concentrations at both sites (WR6: slope = 0.79, r^2 = 0.96, $p < .0001$; WRK: slope = 0.96, r^2 = 0.99, $p < .0001$) (Fig. 5C). Both $(Ca + Mg)_{ex}$ and SO_4 concentrations generally increase with distance from the river at both pore water sites.

Watson River $d^{18}O$ and dD values are low relative to regional precipitation and most pore waters, which decrease with depth in the sediment (Fig. 6). Pore water, precipitation, and river water are all lower and plot closer to the global meteoric water line relative to waters from a nearby nonglacial watershed.

3.2. *Temperature and specific conductivity of pore water*

Time series measurements show systematic variations away from the river as well as diurnal variations of most chemical and hydrologic variables (Fig. 7). Daily maximum pore water temperature lags daily maximum air temperature at all

piezometers (Fig. 7A) and decreases with distance from the river (Fig. 7C). The temperature variations are out of phase with the river water variations, but in phase with the river elevation. The large increase in river elevation on 12 July corresponds with a drop of ~6 °C to near river values in temperature at piezometer B.

The SpC probe in piezometer B failed, but CTDs at piezometers D and E recorded the greatest SpC values and greatest variation of all sites: piezometer D decreases from 172 to 78 lS/cm over the week-long deployment, while piezometer E increases from 136 to 201 lS/cm over the same time period (Fig. 7D). The increase in SpC at piezometer E coincides with the increase in river elevation recorded on 12 July (Fig. 7D). Similarly, the river CTD recorded a subtle decrease in average SpC from 15 to 12.5 lS/cm, corresponding with an increase in river elevation. Minor diurnal variations in SpC are present at all sites (Fig. 7E), although muted compared to the magnitude of change in SpC over the sampling period. Detrended SpC data (Fig. 7E) was produced by subtracting the best fit line of unmodified SpC data in MATLAB. These detrended data show piezometer A varies diurnally from 11 to 17 lS/cm. Piezometer C varies diurnally from 57 to 76 lS/cm, although the maxima are offset from the river by ~12 h.

3.3. *Hydraulic conductivity and discharge/recharge to banks*

Average K_{sat} is greater by an order of magnitude at WR6 (aver- age = 2.2 ± 0.64 x 10^{-4} m/s) than at WRK (average = 4.9 ± 3.7 x 10^{-5} m/s) (Table 1). These values lie within the range of K_{sat} reported in other glaciofluvial environments and moraine sediments (Cooper et al., 2002; Schwartz and Zhang, 2003). No pattern exists between distance from river and magnitude of K_{sat}.

Head gradients were oriented from the Watson River channel toward the bank during the week-long CTD deployment for all locations except piezometer B where head gradients changed orientation on a diurnal basis (Fig. 7B). In the following discussion, head gradients oriented toward the river channel will be positive and indicate discharge from the sediment and away from the river will be negative and indicate recharge to the bank. The diurnal variation in head gradients is out of phase with the river elevation: daily minimum river water elevation corresponds

to daily maxi- mum head gradient. The maximum head gradients lead the mini- mum river elevation, while the minimum (negative) head gradients lead the maximum river elevations by several hours up to the large negative dh/dL deflection and rise of ~15 cm in river elevation on 12 July (Fig. 7)

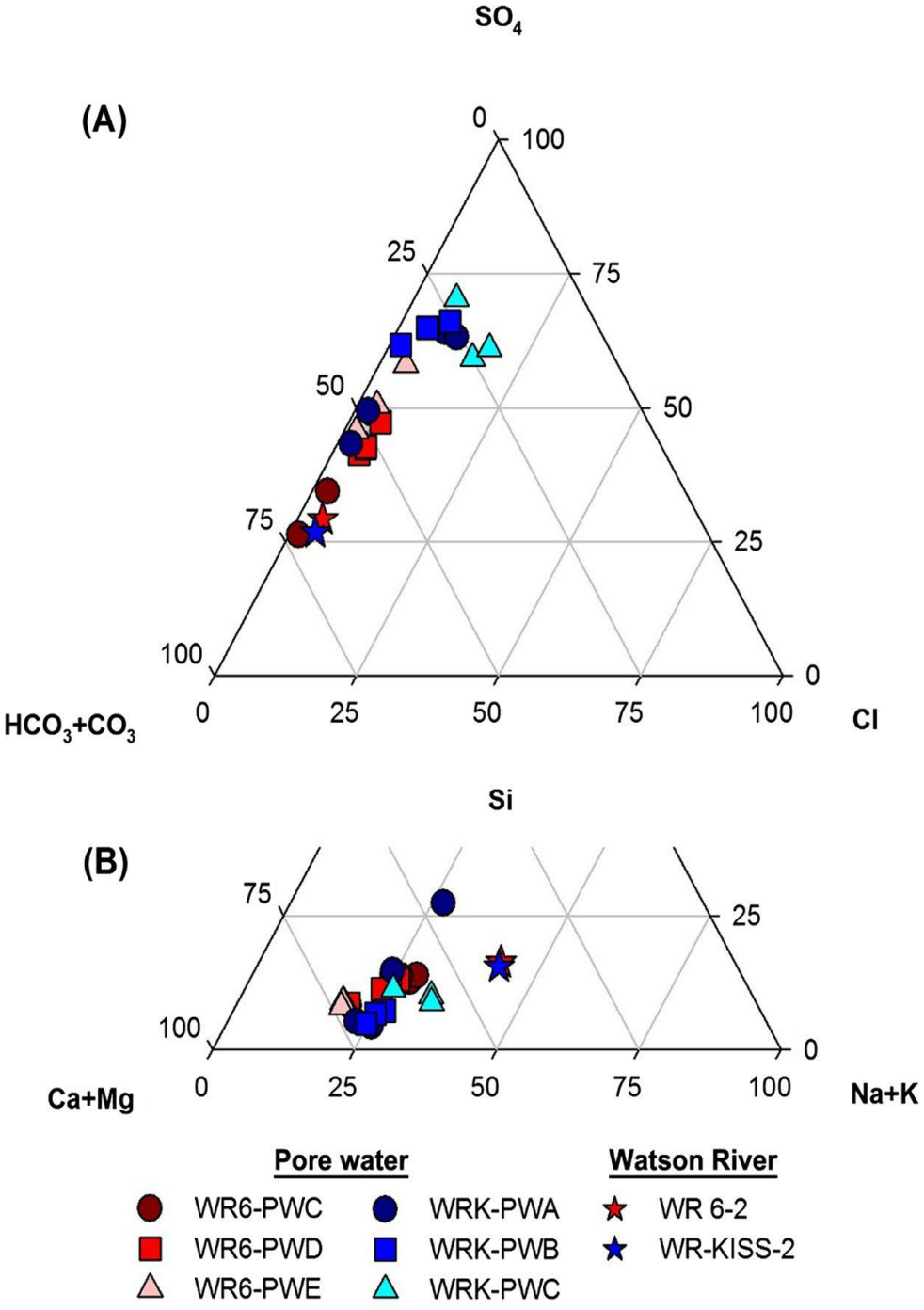

Fig. 3. Ternary diagrams showing relative abundances of A) anions calculated from milliequivalents, and B) cations and silica calculated from millimolar values.

Based on Darcy's law (Eq. (3)), estimated average flow away from the river is 9.8×10^{-8}, 4.2×10^{-8}, and 7.6×10^{-8} m^3/sec at piezometers C, D, and E, respectively over the sample period. At piezometer B, the average net flow (recharge plus discharge) is 8.3×10^{-8} m^3/sec into the river bank, with a recharge value of 1.4×10^{-7} m^3/sec and discharge of 5.4×10^{-8} m^3/sec. Multiplying these average discharge and recharge values by the length of observation, around 6.7 days, yields the total flux into the sediment per m^2 of the river bottom: 5.6×10^{-2}, 2.4×10^{-2}, and 4.4×10^{-2} m^3 per m^2 of river channel at piezometers C, D, and E, respectively. At piezometer B, the total net flow per m^2 of the river bottom is 4.8×10^{-2} m^3, with total recharge of 7.9×10^{-2} m^3 and discharge of 3.1×10^{-2} m^3. Assuming net flow at piezometer B is similar across the Sandflugtdalen, with an approximate wetted river bottom of around 5.2 km^2, the total flow into the river bank over the study period is 2.5×10^5 m^3.

4. Discussion

Specific conductivity values, which reflects solute concentrations, are four to ten times greater in pore water relative to river water (e.g., Fig. 2A), indicating extensive diagenetic reactions occur in sandur sediments. Reactions that alter the pore water chemistry could control fluxes of solutes to the river depending on the reaction and exchange rates. Consequently, fluxes to the river will also depend on the hydrogeologic characteristics of the sediments and head gradients, which control hydrologic exchange flows between river and pore water (e.g.,Harvey and Gooseff, 2015). Therefore, in the following discussion, we evaluate potential sources of water to the active layer adjacent to the river, define reactions that could alter the pore water compositions, estimate potential exchanges between the river and pore waters, and speculate on potential changes in solute fluxes that may result from this exchange.

4.1. Sources of water to the active layer

Sources to sandur pore water in addition to Watson River water could include flow from deep groundwater or proximal non-glacial watersheds (i.e., those watersheds separated from the ice sheet by hydrologic divides; Scribner et al., (2015)), active layer

melt, and precipitation. Deep groundwater exists along fractures in bedrocks, but is separated from active layer groundwater and surface water by continuous permafrost (Nielsen, 2010). Small non-glacial (deglaciated) tributaries enter the Watson River along its length, but the magnitude of this discharge is minimal compared to ice- derived drainage (Aebly and Fritz, 2009; Ryu and Jacobson, 2012). Numerous lakes surround the Watson River watershed, but all are separated from the watershed by topographic highs pre- venting their discharge to the river. Therefore, the most likely source of pore water, other than the Watson River, is direct recharge from annual precipitation, despite the negative water balance.

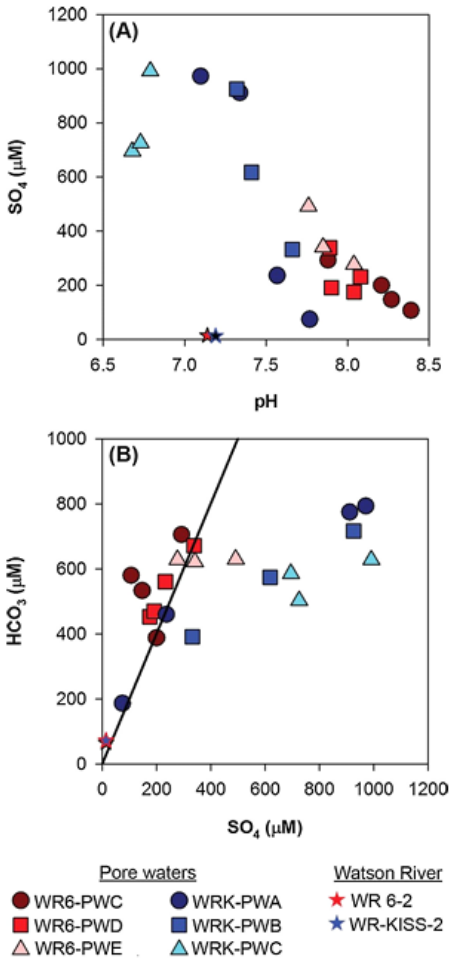

Fig. 4. Geochemical relationships between river and pore waters. A) pH versus SO4 concentrations, B) SO4 versus HCO3 concentrations (solid line is the 2:1 molar relationship expected from sulfide oxidation coupled to carbonate dissolution). Blue star with red outline indicates overlapping Watson River data. (For interpretation of the references to colour in this figure legend, the reader is referred to the web version of this article.)

Given high K_{sat} values compared to other media (Table 1; Schwartz and Zhang, 2003), direct recharge by precipitation should be rapid when it occurs, thereby limiting immediate evaporation. Mixing between water recharged through the land surface and exchanged with the Watson River is shown by stable isotope ratios that are bracketed by Watson River water and precipitation (Fig. 6). Pore water ^{18}O and δD values in sediment near the river trend toward Watson River values, while pore water farther from the river has values closer to those of precipitation, reflecting a gradient in mixing proportions of river water and recharged precipitation. Additional precipitation could recharge the sandur from surrounding highlands because the orthogonal land surface slope to the river along the sandurs is two orders of magnitude greater than the longitudinal slope.

4.2. *Geochemical processes in river versus pore water*

Pore water solute concentrations generally increase with distance from the river (Fig. 7D) and depth (Fig. 2A), consistent with other permafrost-affected rivers (e.g., Cooper et al., 2002; Gooseff et al., 2013, 2003; Ward et al., 1999). This distribution of solutes could reflect two end-member conditions: either little hydrologic exchange coupled with long pore water residence times that allow extensive weathering reactions, or active hydrologic exchange associated with rapid weathering. Both of these end-member processes likely occur and their relative magnitudes likely evolve through the melt season, depending on temperature and river discharge conditions. The rates of weathering reactions depends on mineralogical compositions of outwash sediments, which reflect comminuted and homogenized bedrock. Bedrock of the NMB consists predominantly of quartz and feldspars along with minor amounts of mica, calcite, pyrite, and heavy minerals (Hindshaw et al., 2014). Although sediment compositions are dominated by silicate minerals, the dominant pore waters reactions are carbon- ate dissolution and sulfide oxidation (e.g., reactions (4)–(6)) based on low relative Si concentration and elevated SO_4 concentrations (Fig. 3), similar to alpine proglacial catchments (e.g., Anderson, 2007) and surrounding deglaciated watersheds (Scribner et al., 2015). Other secondary mineral precipitates (e.g., reaction (8)) must also be considered in

the pore water chemistry because summer evaporation and winter cryoconcentration can lead to precipitation of evaporite minerals (Barrett et al., 2009; Cooper et al., 2002; Killawee et al., 1998; Tranter, 2003).

4.2.1. ***Preferential weathering***

Both sulfuric and carbonic acid may drive weathering. Watson River water HCO_3:SO_4 ratios >2 indicate carbonic acid weathering dominates in the river e.g., (Tranter et al., 2002). Hydration of atmospheric CO_2 is the most likely source of the carbonic acid as little dissolved organic carbon is available for remineralization in Greenland Ice Sheet proglacial rivers (Bhatia et al., 2013; Lawson et al., 2014). Carbonic acid also controls weathering in the pore water at WR6 where HCO_3:SO_4 ratios are 22. At WRK, however, where HCO_3:SO_4 ratios are <2, sulfide mineral oxidation and pro- duction of sulfuric acid or dissolution of sulfate salts may con- tribute SO_4 (Fig. 4B). The inverse correlation between pH and SO_4 concentrations supports oxidation of sulfide minerals and production of sulfuric acid (Figs. 3A and 4A), which could enhance both carbonate and silicate mineral weathering (e.g., Tranter, 2003).

At WRK, low pH and HCO_3:SO_4 ratios (Fig. 4) suggest the loss of easily weathered carbonate minerals that would buffer pH. This loss of carbonate could occur as sediments pass through multiple sandurs on their journey downstream, increasing their residence time in the system. A similar shift from predominately carbonate dissolution to sulfide oxidation occurs with increasing exposure age and rainfall in deglaciated watersheds in a transect from Kangerlussuaq to Sisimiut in western Greenland (Scribner et al., 2015). The preferential removal of trace carbonate minerals from the sandur sediment reflects the large scale weathering evolution across glacial landscapes (Anderson et al., 2000; Scribner et al., 2015) and suggests that much of this weathering could occur in pore water of sandur sediments of proglacial rivers.

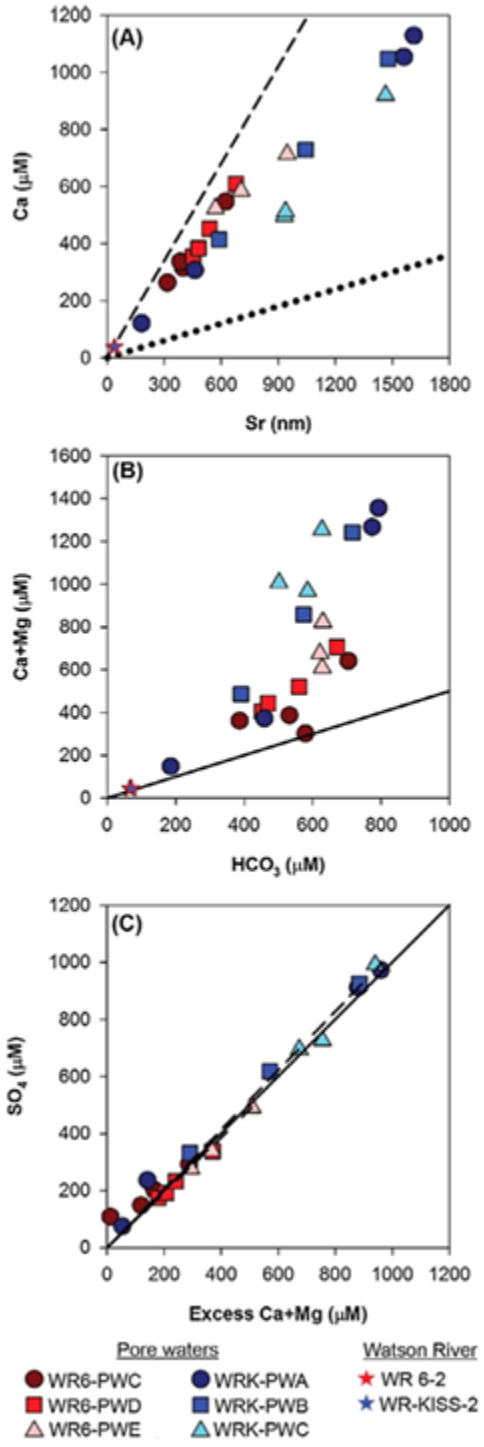

Fig. 5. A) Sr versus Ca concentrations. Endmember silicate (dotted line, slope = 0.18) and carbonate (dashed line, slope = 0.88) trends for the region are included. B) HCO_3 versus Ca + Mg concentrations. Solid line is the molar relationship expected from Ca- Mg carbonate or silicate dissolution (slope = 0.5). C) Dissolved SO_4 versus excess Ca + Mg concentrations present in excess of carbonate or silicate weathering. Solid line is the 1:1 Ca:SO_4 molar ratio associated with the dissolution of gypsum. Dashed lines are regression lines for WR6 pore waters (slope = 0.97) and WRK pore waters (slope = 0.79). Blue star with red outline indicates overlapping Watson River data.

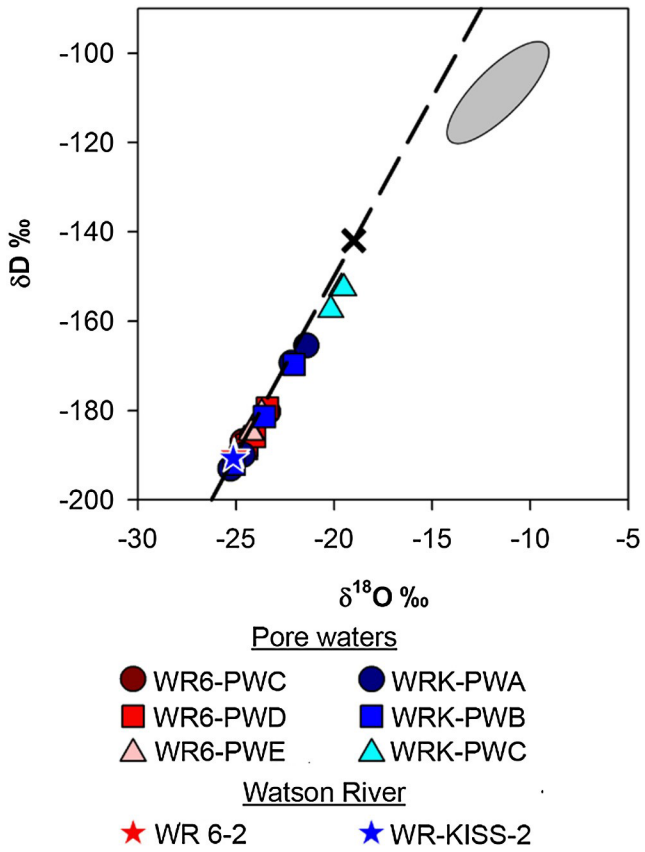

Fig. 6. $d^{18}O$ versus dD for Watson River water, pore water, and a flowing deglacial watershed in the Kangerlussuaq region (this study). Gray ellipse represents water isotope values for a nonglacial watershed in the Kangerlussuaq region. Black 'X' is the mean weighted precipitation value for the Kangerlussuaq area from Leng and Anderson (2003). Dashed line is the global meteoric water line.

The relative impact of silicate versus carbonate mineral weathering can be assessed by comparing Ca:Sr ratios because these two mineral groups have distinct proportions of Ca:Sr (Scribner et al., 2015). We compare Sr and Ca ratios with regional end-members for silicate and carbonate mineral weathering derived from analysis of Watson River bedload material. Silicate minerals in the region have an average Ca:Sr ratio of 0.18 mmol/nmol, while carbonate minerals, as inferred from a weak acid leachate of bedload sediments, have an average Ca:Sr ratio of 0.88 mmol/nmol. Carbonate weathering appears to dominate the Watson River considering Ca:Sr ratios are 0.99 at WR6 and 0.95 at WRK (Appendix 2), which is consistent with alpine glacial systems (e.g., Anderson, 2007). These findings are also consistent with Ryu and Jacobson (2012), who estimate 28–68% of cations in Watson River water are due to carbonate weathering. However, Wimpenny et al. (2011) estimated only 2–14%

of solutes in the Watson are due to carbonate weathering based on d26Mg composition, while Yde et al. (2014) dismiss carbonate weathering as a major source of solutes based on Ca:Na and Mg:Na that cluster near silicate rock compositions. In contrast with Watson River water, WR6 and WRK pore waters have average Ca:Sr ratios of 0.84 ± 0.05 μM/nM and 0.65 ± 0.06 μM/nM, respectively (Appendix 1), reflecting both more silicate weathering in the pore water than river water and a downstream increase in pore water silicate weathering. Both of these processes reflect the loss of easily weathered carbonate minerals with long residence times in the river. In addition, the increase in silicate weathering at WRK over WR6 could reflect hydrologic control because the order of magnitude greater average Ksat values at WR6 than WRK (Table 1) could slow hydrologic exchange flows.

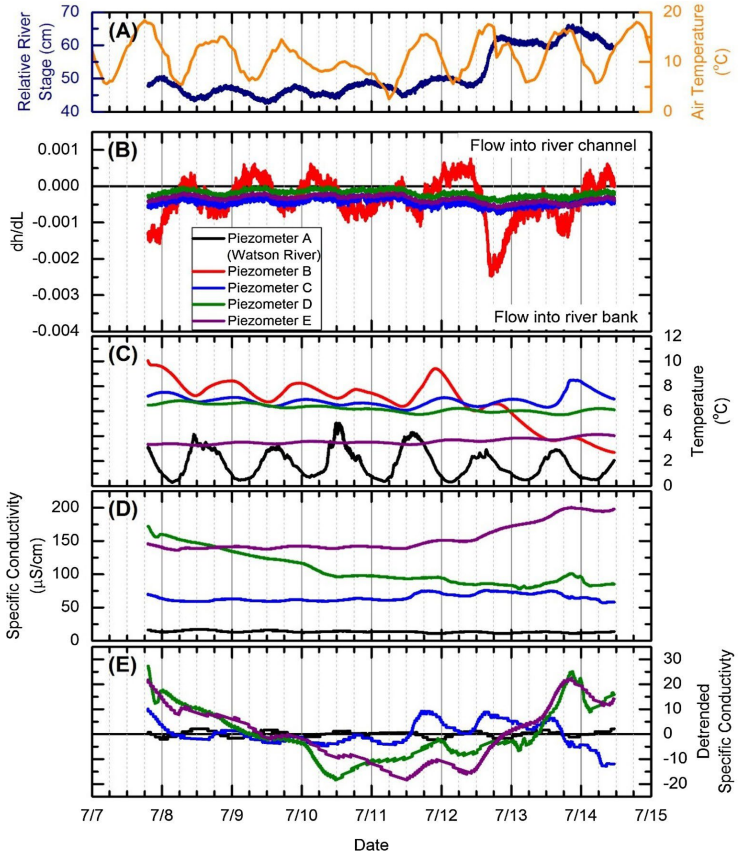

Fig. 7. Hydrologic data from week-long CTD deployment at WR6. A) Relative river stage calculated from pressure reading in piezometer A (dark blue) and local air temperature (orange) from Cappelen (2014); B) head gradient (dh/dL) indicating direction of flow: positive from stream bank to channel, negative from channel to stream bank; C) temperature; D) specific conductivity (SpC); E) linear detrend (see text) of specific conductivity data to better show diurnal variation. Specific conductivity sonde for piezometer B failed prior to deployment, thus no data are presented. Pore water sampling occurred several meters upstream shortly after CTDs were removed. Large ticks with dates indicate midnight.

Table 1 Hydraulic conductivity by location

	Distance from channel (m)	K_{sat} (m/s)	Standard Deviation (m/s)
Sandflugtdalen*		**2.2×10^{-4}**	
WT6-PWC	6.0	2.0×10^{-4}	1.5×10^{-5}
WR6 PWD	9.5	2.9×10^{-4}	3.4×10^{-5}
WR6-PWE	13.5	1.7×10^{-4}	5.8×10^{-5}
KISS*		**4.9×10^{-5}**	
WRK-PWA	2.5	9.1×10^{-5}	2.1×10^{-5}
WRK-PWB	6.0	2.3×10^{-5}	5.6×10^{-6}
WRK-PWC	9.5	3.2×10^{-5}	3.6×10^{-6}

*Bold values represent average.

Both the change in minerals weathered and acids involved in weathering could alter how proglacial river systems affect the global carbon cycle. Silicates weathered by sulfuric acid do not play a role in the global carbon cycle, but silicates weathered by carbonic acid represent a net sink of atmospheric CO_2 (Berner et al., 1983), while carbonate minerals weathered by sulfuric acid represent a net source of CO_2 to the atmosphere (Galy and France-Lanord, 1999; Martin, 2017; Ryu and Jacobson, 2012). Downstream carbonic acid weathering of silicate and carbonate minerals in the Watson River sequesters 75% of dissolved CO_2 (Ryu and Jacobson, 2012). Even in granitoid terrains where carbonates are rare, carbonates weather preferentially relative to silicates (Anderson, 2007; White et al., 2005, 1999). The increase in SO_4 and decrease in pH suggest that sulfuric acid weathering of carbonate in the pore water would increase pCO_2 of the pore water, and that the generated CO_2 could be transferred to the river with hydrologic exchange flow.

4.2.2. *Influence of evaporation/cryoconcentration*

In addition to mineral weathering reactions, pore water compositions can be modified by evaporation and cryoconcentration. Evaporative concentration, which is enhanced by the negative water balance in the region (Hasholt and Sogaard, 1978;

Nielsen, 2010), increases solute concentrations. This concentration mechanism affects the portion of the water table near the land surface where capillary action moves shallow groundwater toward the land sur- face (Barrett et al., 2009; Tranter, 2003). During the winter, cryoconcentration increases solutes at depth by surface-down and permafrost-up active layer freeze-in (Cooper et al., 2002; Tranter, 2003). Both evaporation and cryoconcentration could precipitate secondary minerals including calcite and sulfate salts in water contained in the active layer, regardless of whether such precipitation occurs in the phreatic zone or meniscus water in the vadose zone (Cooper et al., 2002; Killawee et al., 1998; Tranter, 2003). The region lacks primary evaporite deposits at the surface to contribute to water compositions (Ryu and Jacobson, 2012). Although gypsum has been found at depths >300 m (Pere, 2014), continuous permafrost limits the interaction with active layer pore waters (Nielsen, 2010). Therefore, the primary source of SO_4 in these systems must be the oxidation of sulfide minerals in the sub- or pro- glacial environments. Precipitation of sulfate salts by freezing or evaporation could then concentrate the sulfate during subsequent dissolution by melt waters during the summer thaws (Tranter, 2003).

Dissolution of secondary Ca-Mg sulfate salts is reflected in pore water with Ca + Mg concentrations in excess of those expected from silicate or carbonate weathering (Fig. 5B) assuming a $(Ca + Mg)_{ex}$:SO_4 ratio of 1 (Fig. 5C). Dissolution is likely as pore water samples are undersaturated with respect to both calcite and gyp- sum (Appendix 1 and 2). Excess Ca + Mg concentrations increase away from the river (Fig. 5C), similar to the SpC values (Fig. 7D), indicating alteration of pore water compositions by evaporation and cryoconcentration. The $(Ca + Mg)_{ex}$ concentration in the pore water represents 2–56% of the total cation concentration, making it a substantial contributor to its composition. Assuming all excess Ca and Mg present in pore water is due to the dissolution of secondary gypsum, 2–165 mg of gypsum per liter of water must dis- solve to reach current pore water concentrations. Solute concentrations that increase with distance from the river (Figs. 2A and 7D) suggest that hydrologic exchange flow diminishes with distance from the channel, at least over the sampling period, and evapoconcentration increases solute concentrations similar to streams in the dry valley of Antarctica (Gooseff et al.,

2003) and at Finsternwalderbreen in Svalbard (Cooper et al., 2002). However, the relationship between increased solute concentrations in pore waters with distance from the river could also depend on the river stage. As sandurs flood with increased melting and discharge, hydrologic exchange flows could alter pore water concentrations. Because we sampled only over a short period, we are unable to quantitatively assess the impact of seasonal flooding of the sandurs.

4.3. *Evidence for river-pore water exchange and storage*

Glacial meltwater streams have unsteady flow due to pulses of glacial melt at diurnal frequencies (e.g., Koch et al., 2011; Runkel et al., 1998) and through the melt season (e.g., Hasholt et al., 2013). This variable flow alters head gradients and direction and magnitudes of hydrologic exchange flows. Peak Watson River discharge at Søndre Strømfjord lags peak ice sheet melt by ~10 h (Hasholt et al., 2013) and causes the ~6 h lag in river stage and peak air temperature at WK6 (Fig. 7A). The diurnal variations in river stage result in periodic changes between positive and negative head gradient values at piezometer B, and indicate water alter- nates between flow into and out of the bank. This periodic reversal of flow ceased on 12 July when river stage rose over a ~6 h period and increased the head gradient by more than the diurnal head gradient fluctuations (Fig. 7B). This change was not from local precipitation as <1 mm of rain fell during 7–14 July (Cappelen, 2014). Rather, rising stage resulted from changes in the magnitude of regional glacial melt and/or the reorganization of the subglacial hydrological system (e.g., Bartholomew et al., 2011; Chandler et al., 2013; Graly et al., 2017). This increase was documented by increased discharge at an upstream gauging station (Rennermalm et al., 2014). The increase in stage caused flow into the bank for ~30 h and flow of river water into the bank is supported by a simultaneous decrease in temperature at piezometer B from ~8°C to near river values of ~3 °C (Fig. 7C). Although this event occurred near the end of our record, it appears the system equilibrated and returned to diurnal positive head gradients at piezometer B while at a higher overall stage (Fig. 7).

Negative head gradients at the distal piezometers (C, D, and E) indicate a flow direction always away from the river outside of the zone with hydrologic exchange

flows (Fig. 7B). These head gradients reflect the overall increase in river stage during the sampling period. The distal piezometers also did not record the overall decrease in temperature corresponding with the rise in river stage on 12 July, further indicating river water did not reach these piezometers (Fig. 7C). Furthermore, SpC values recorded at the distal piezometers never approach river water values (Fig. 7D). Instead, the SpC records reflect flow away from the river consistent with the negative head gradients. Over the period of record, SpC at piezometer D decreases from ~175 µS/cm to near piezometer C values of ~50 µS/cm and piezometer E increases from ~150 µS/cm to values similar to the initial piezometer D value of ~175 µS/cm. These trends suggest low conductivity water flowed from piezometer C to D, while high conductivity water flowed from D to E. However, flow away from the river is modified by diurnal variations in river stage, as reflected in dh/dL values that vary in phase with dh/dL observed at piezometer B (Fig. 7B).

The Watson River is ungauged at the Sandflugtdalen so we lack information on the discharge during our observations. Although average discharge into Søndre Strømfjord is 117 m^3/sec (Hasholt et al., 2013) which includes discharge from a proglacial drainage of about equal size to the Watson River and suggests that discharge upstream of the confluence would be around half the total discharge or around 60 m^3/sec. Watson River discharge was measured upstream of Sandflugtdalen to be around 9 m^3/sec (Rennermalm pers. comm, 2017). Using these two values as bounds on flow through Sandflugtdalen, the total volume of river water discharged was between 5.2 and 35 x 10^6 m^3. Comparing this value with estimates of total water lost to the sediment during our period of observation; approximately 1–8% of the river flow recharged the river bank.

4.4. *Implications for hydrologic exchange flows and solute fluxes*

Over the study period, hydrologic exchange flow between river and pore water was limited to within a few meters of the river channel, and depends on river flow. River discharge varies diurnally driving proximal exchange in (Fig. 8A) and out (Fig. 8B) of the bank near the channel.

Rapid changes in discharge, such the event on 12 July, temporarily flood the

river bank providing dilute river water recharge to distal pore waters that evolve by carbonate dissolution, sulfide oxidation, and further dissolution of secondary salts. Farther from the river, the flow direction is always away from the channel, which isolates the water (e.g., Gooseff et al., 2003) and alters the pore water compositions through carbonate dissolution, sulfide oxidation, and dissolution of secondary salts. The isolation of this water is reflected in increasingly altered compositions with distance from the river (Fig. 2A).

While the present data set cannot constrain hydrologic exchange flows and geochemical evolution of pore and river waters on a seasonal timescale, over the course of the melt season, changes in discharge could drive conditions similar to those we observed at diurnal frequency (Fig. 8). However, as changing melt conditions change river channel location (e.g., channel migration, curvature, etc.) could also affect the timing and location of dilute river water infiltration into the subsurface that cannot be predicted by our data. Since river discharge depends on ice sheet conditions, areas of the sandur could be inundated one year but not in subsequent years, effectively trapping water in the subsurface despite the high K_{sat} of sediment in the outwash plain. Thus, low water- rock ratios, relatively high K_{sat}, and long subsurface flow paths allow weathering to alter the pore water compositions.

The diurnal variations in head gradients and known variations in discharge also allow us to predict that distal exchange could be seasonally important to the solute load of the Watson River. Seasonal variations in river stage should allow surface water to infiltrate the subsurface during high discharge and pore waters to flow to the river during low discharge (e.g., Koch et al., 2011). Lower river discharge occurs early and late in the melt season and correlates to cooler temperatures and a decrease in glacial melt. At these times, regional head gradients should be oriented toward the river channel, causing flow of pore waters into the river. This flow will be modified by the extent of thaw-out or freeze-in of the active layer and the heterogeneity of sandur sediment. The discharge could be on the same order of magnitude as the recharge, estimated here to be around 1–8% of the total river flow, although pore water volumes could be modified by evaporation or direct recharge.

Because the chemical compositions of the pore water are four to ten times greater than the river, even this small discharge relative to the river flow could impact the river water chemistry and solute fluxes.

Currently, proglacial watersheds provide ~0.6–1% of global run- off to the ocean; the Greenland Ice Sheet is responsible for approximately one-third of modern proglacial runoff (Tranter, 2003). As the climate warms and enhanced melting continues, solute fluxes to the ocean are also expected to increase. For example, discharge from ice sheets provides a significant source of bioavailable and particulate iron to coastal oceans, and is also expected to increase as discharge increases (Bhatia et al., 2013; Hawkings et al., 2014). As active layer thaw depths increase in a warming climate, the volume of the subsurface available for reaction will also increase, though the hydrologic exchange flow is not limited by active layer depth during peak melt (Edwardson et al., 2003). The extent of hydrologic exchange flow should increase until a threshold depth is reached as determined by head gradients and stream morphology (Zarnetske et al., 2008). However, the significance of these fluxes will be modulated by the magnitude of discharge in the Watson River as melting becomes more extensive.

5. Conclusions

This study provides an initial assessment of hydrologic exchange flows in a proglacial river draining the Greenland Ice Sheet and potential solute fluxes based geochemistry of surface and pore waters and hydrogeologic observations. The relative importance of sulfuric acid compared to carbonic acid to weathering increases downstream and solute compositions indicate carbonate weathering dominates relative to silicate weathering in both river and pore water. These shifts in weathering acid and weathered minerals will impact drawdown of atmospheric CO_2. Although this study only represents a snapshot of the dynamics of river-pore water exchange, pore water solute concentrations that are elevated over those in the river, and high K_{sat} of bank sediments highlight the potential for solute fluxes from the bank, through the river, and ultimately to the ocean from the proglacial watershed. Hydrologic exchange flows were limited to within ~6 m of the river channel at the time of observation, and narrowed with increasing discharge. This flow reversed

direction at diurnal periodicity because of diurnal variations in the river stage. In contrast, head gradients were always oriented away from the river, although with diurnal variation in magnitude, indicating continuous flow away from the river channel. Pore water far from the river should therefore flow to the river only during periods of low river stage. These preliminary observations indicate that weathering of extensive sediment deposits in sandurs are likely important contributors to proglacial river water compositions. Weathering in sandur pore waters could thus have an important impact on ocean water chemistry during continental ice sheet melting and may impart a seasonal signal in the discharge of solutes.

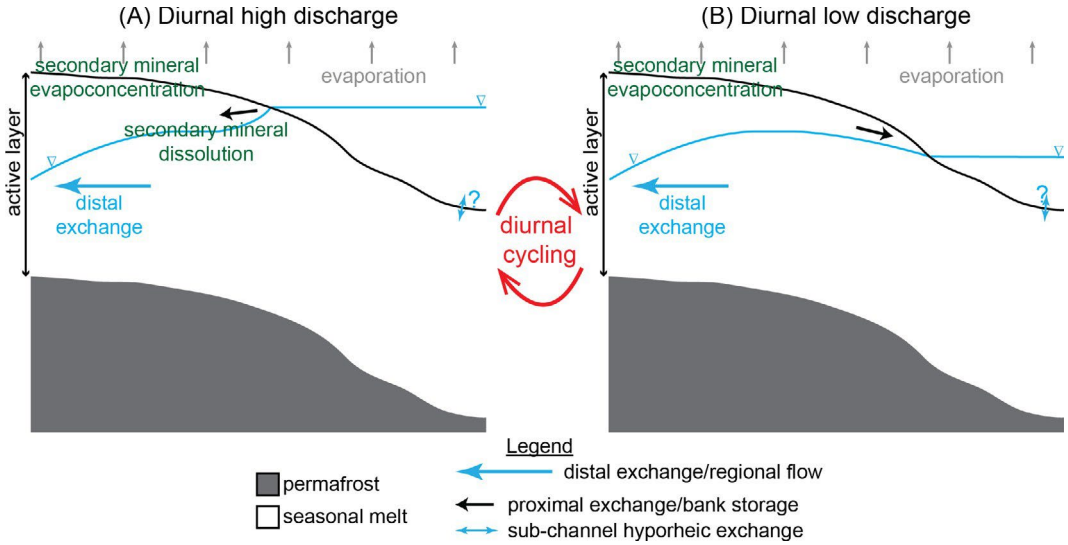

Fig. 8. Conceptual model of exchange between Watson River and adjacent pore waters through the melt season during the study period. See text for detail. A) Diurnal high discharge conditions and B) diurnal low discharge conditions.

Acknowledgements

Financial support for this study is from NSF Grant # ARC- 1203773 and PLR-1603452 to JBM and EEM, National Geographic Society Committee for Research and Exploration Grant #9076-12 to JBM and Young Explorer Program Grant #9121-12 to KMD. This work was conducted under Export license 027/2013 from the Bureau of Minerals and Petroleum, Government of Greenland, which we gratefully acknowledge. We thank G. Kamenov and J. Curtis for their help with sample analyses, as well as D. Collazzo, M. Davlantes, and A. Portier for their help with fieldwork and sample

collection. We also thank Dr. Todd C. Rasmussen and an anonymous reviewer for their thoughtful comments that helped to improve this manuscript.

Appendix A. Supplementary data

Supplementary data associated with this article can be found, in the online version, at https://doi.org/10.1016/j.jhydrol.2017.11. 002.

References

Aebly, F.A., Fritz, S.C., 2009. Palaeohydrology of Kangerlussuaq (Sondre Stromfjord), west Greenland during the last ~8000 years. Holocene 19, 91–104.

Anderson, S.P., Drever, J.I., Frost, C.D., Holden, P., 2000. Chemical weathering in the foreland of a retreating glacier. Geochim. Cosmochim. Acta 64, 1173–1189.

Anderson, S.P., 2007. Biogeochemistry of Glacial Landscape Systems. Annu. Rev. Earth Planet. Sci. 35, 375–399.

Anderson, S.P., Drever, J.I., Humphrey, N.F., 1997. Chemical weathering in glacial environments. Geology 25, 399–402.

Barrett, J.E., Gooseff, M.N., Takacs-Vesbach, C., 2009. Spatial variation in soil active- layer geochemistry across hydrologic margins in polar desert ecosystems. Hydrol. Earth Syst. Sci. Discuss. 6, 3725–3751.

Bartholomew, I., Nienow, P., Mair, D., Hubbard, A., King, M.a., Sole, A., 2010. Seasonal evolution of subglacial drainage and acceleration in a Greenland outlet glacier. Nat. Geosci. 3, 408–411. https://doi.org/10.1038/ngeo863.

Bartholomew, I., Nienow, P., Sole, A., Mair, D., Cowton, T., Palmer, S., Wadham, J., 2011. Supraglacial forcing of subglacial drainage in the ablation zone of the Greenland ice sheet. Geophys. Res. Lett. 38, 1–5. https://doi.org/10.1029/ 2011GL047063.

Berner, R.A., Lasaga, A.C., Garrels, R.M., 1983. Carbonate-silicate geochemical cycle and its effect on atmospheric carbon dioxide over the past 100 million years. Am. J. Sci. 283, 641–683.

Bhatia, M.P., Kujawinski, E.B., Das, S.B., Breier, C.F., Henderson, P.B., Charette, M.a., 2013. Greenland meltwater as a significant and potentially bioavailable source of iron to the ocean. Nat. Geosci. 6, 274–278.

Boulton, A.J., Findlay, S., Marmonier, P., Stanley, E.H., Valett, H.M., 1998. The functional significance of the hyporheic zone in streams and rivers. Annu. Rev. Ecol. Syst. 29, 59–81.

Bouwer, H., 1989. The Bouwer and Rice slug test – an update. Ground Water 27, 304–309.

Bouwer, H., Rice, R.C., 1976. A slug test for determining hydraulic conductivity of unconfined aquifers with completely or partially penetrating wells. Water Resour. Res. 12, 423–428.

Cappelen, J., 2014. Weather observations from Greenland 1958-2013 – observation data with description. Copenhagen.

Cappelen, J., Jørgensen, B.V., Laursen, E.V., Stannius, L.S., Thomsen, R.S., 2001. The Observed Climate of Greenland, 1958-99 – with Climatological Standard Normals, 1961-90.

Chandler, D.M., Wadham, J.L., Lis, G.P., Cowton, T., Sole, A., Bartholomew, I., Telling, J., Nienow, P., Bagshaw, E.B., Mair, D., Vinen, S., Hubbard, A., 2013. Evolution of the subglacial drainage system beneath the Greenland Ice Sheet revealed by tracers: supplementary information. Nat. Geosci. 6, 195–198.

Charette, M.a., Allen, M.C., 2006. Precision ground water sampling in coastal aquifers using a direct-push, shielded-screen well-point system. Ground Water Monit. Rem., 26, pp. 87–93.

Cooper, R.J., Wadham, J.L., Tranter, M., Hodgkins, R., Peters, N.E., 2002. Groundwater hydrochemistry in the active layer of the proglacial zone, Finsterwalderbreen, Svalbard. J. Hydrol. 269, 208–223.

Crocket, K.C., Vance, D., Foster, G.L., Richards, D.A., Tranter, M., 2012. Continental weathering fluxes during the last glacial/interglacial cycle: insights from the marine sedimentary Pb isotope record at Orphan Knoll, NW Atlantic. Quatern. Sci. Rev. 38, 89–99. https://doi.org/10.1016/j.quascirev.2012.02.004.

Dijkmans, J.W.A., Tornqvist, T.E., 1991. Modern periglacial eolian deposits and landforms in the Søndre Strømfjord area, West Greenland and their palaeoenvironmental implications. Meddelelser om Grønland Geosci. 25, 3–39.

Edwardson, K.J., Bowden, W.B., Dahm, C., Morrice, J., 2003. The hydraulic characteristics and geochemistry of hyporheic and parafluvial zones in Arctic tundra streams, north slope, Alaska. Adv. Water Resour. 26, 907–923.

Escher, A., Watt, W.S., 1976. Geology of Greenland. Grønlands Geologiske undersøgelse, Copenhagen.

Galy, A., France-Lanord, C., 1999. Weathering processes in the Ganges-Brahmaputra basin and the riverine alkalinity budget. Chem. Geol. 159, 31–60.

Gooseff, M.N., Barrett, J.E., Levy, J.S., 2013. Shallow groundwater systems in a polar desert, McMurdo Dry Valleys, Antarctica. Hydrogeol. J. 21, 171–183.

Gooseff, M.N., McKnight, D.M., Runkel, R.L., Vaughn, B.H., 2003. Determining long time-scale hyporheic zone flow paths in Antarctic streams. Hydrol. Process. 17, 1691–1710.

Graly, J., Harrington, J., Humphrey, N., 2017. Combined diurnal variations of discharge and hydrochemistry of the Isunnguata Sermia outlet of the Greenland Ice Sheet give in sight on sub glacial conditions. Cryosphere, 1131–1140.

Harvey, J., Gooseff, M., 2015. River corridor science: hydrologic exchange and ecological consequences from bedforms to basins. Water Resour. Res. 51, 6893– 6922. https://doi.org/10.1002/2015WR017617.

Hasholt, B., Bech Mikkelsen, A., Holtegaard Nielsen, M., Andreas Dahl Larsen, M., 2013. Observations of runoff and sediment and dissolved loads from the Greenland Ice Sheet at Kangerlussuaq, West Greenland, 2007 to 2010. Zeitschrift für Geomorphologie, Supplem. Issues 57, 3–27.

Hasholt, B., Sogaard, H., 1978. Et Forsog Pa En Klimatiskhydrologisk Regionsinddeling Af Holsteinsborg Kommune (Sisimiut). Geografisk Tidsskrift-Danish J Geogr. 77, 72–92.

Hawkings, J., Wadham, J., Tranter, M., Telling, J., Beaton, A., Simmons, S., Chandler, D., Tedstone, A., Nienow, P., 2016. The Greenland Ice Sheet as a hotspot of phosphorus weathering and export in the Arctic. Global Biogeochem. Cycles 30, 191–210. https://doi.org/10.1002/2015GB005237.

Hawkings, J.R., Wadham, J.L., Tranter, M., Raiswell, R., Benning, L.G., Statham, P.J., Tedstone, A., Nienow, P., Lee, K., Telling, J., 2014. Ice sheets as a significant source of highly reactive nanoparticulate iron to the oceans. Nat. Comm. https://doi.org/10.1038/ncomms4929.

Hawkings, J.R., Wadham, J.L., Tranter, M., Lawson, E., Sole, A., Cowton, T., Tedstone, A.J., Bartholomew, I., Nienow, P., Chandler, D., Telling, J., 2015. The effect of warming climate on nutrient and solute export from the Greenland Ice Sheet. Geochem. Perspect. Lett. 94–104. https://doi.org/10.7185/geochemlet.1510.

Hindshaw, R.S., Rickli, J., Leuthold, J., Wadham, J., Bourdon, B., 2014. Identifying weathering sources and processes in an outlet glacier of the Greenland Ice Sheet using Ca and Sr isotope ratios. Geochim. Cosmochim. Acta 145, 50–71.

Howat, I.M., Negrete, A., Smith, B.E., 2014. The Greenland Ice Mapping Project (GIMP) land classification and surface elevation data sets. Cryosphere 8, 1509– 1518. https://doi.org/10.5194/tc-8-1509-2014.

Killawee, J.A., Fairchild, I.J., Tison, J.L., Janssens, L., Lorrain, R., 1998. Segregation of solutes and gases in experimental freezing of dilute solutions: implications for natural glacial systems. Geochim. Cosmochim. Acta 62, 3637–3655.

Koch, J.C., McKnight, D.M., Neupauer, R.M., 2011. Simulating unsteady flow, anabranching, and hyporheic dynamics in a glacial meltwater stream using a coupled surface water routing and groundwater flow model. Water Resour. Res. 47, W05530. https://doi.org/10.1029/2010WR009508.

Kurzweil, F., Gutjahr, M., Vance, D., Keigwin, L., 2010. Authigenic Pb isotopes from the Laurentian Fan: changes in chemical weathering and patterns of North American freshwater runoff during the last deglaciation. Earth Planet. Sci. Lett. 299, 458–465.

Lawson, E.C., Wadham, J.L., Tranter, M., Stibal, M., Lis, G.P., Butler, C.E.H., Laybourn-Parry, J., Nienow, P., Chandler, D., Dewsbury, P., 2014. Greenland Ice Sheet exports labile organic carbon to the Arctic oceans. Biogeosciences 11, 4015– 4028.

Leng, M.J., Anderson, N.J., 2003. Isotopic variation in modern lake waters from western Greenland. Holocene 13, 605–611.

Malard, F., Tockner, K., Ward, J.V., 1999. Shifting dominance of subcatchment water sources and flow paths in a glacial floodplain, Val Roseg, Switzerland. Arct. Antarct. Alp. Res. 31, 135–150. https://doi.org/10.2307/1552602.

Martin, J.B., 2017. Carbonate minerals in the global carbon cycle. Chem. Geol. 449, 58–72. https://doi.org/10.1016/j.chemgeo.2016.11.029.

Mowatt, T.C., Naidu, A.S., 1994. Petrographic characterization of some Precambrian crystalline rocks from the Sondre Stromfjord area, west Greenland. BLM-Alaska Open File Report 54.

Nezat, C.A., Lyons, W.B., Welch, K.A., 2001. Chemical weathering in streams of a polar desert (Taylor Valley, Antarctica). Bull. Geol. Soc. Am. 113, 1401–1408.

Nielsen, A.B., 2010. Present conditions in Greenland and the Kangerlussuaq area. Work. Rep. 2010–07, 70.

Parkhurst, B.D.L., Appelo, C. a J., 1999. User's Guide To PHREEQC (version 2) — a Computer Program for Speciation, and Inverse Geochemical Calculations. Exchange Organizational Behavior Teaching Journal D, 326.

Pere, T., 2014. Geological Logging of the Greenland Analogue Project Drill Cores DH- GAP01, 03 and 04.

Rennermalm, A.K., Smith, L.C., Chu, V.W., Moustafa, S.E., Pitcher, L., Gleason, C., 2014. Proglacial river dataset from the Akuliarusiarsuup Kuua River northern tributary, Southwest Greenland, 2008 – 2013, version 2.0. doi:10.1594/PANGAEA.838812.

Runkel, R.L., Mcknight, D.M., Andrews, E.D., 1998. Analysis of transient storage subject to unsteady flow: diel flow variation in an antarctic stream. J. North Am. Benthol. Soc. 17, 143–154.

Ryu, J.S., Jacobson, A.D., 2012. CO2 evasion from the Greenland Ice Sheet: a new carbon-climate feedback. Chem. Geol. 320–321, 80–95.

Schwartz, F., Zhang, H., 2003. Fundamentals of Ground Water. John Wiley & Sons Inc.

Scribner, C.A., Martin, E.E., Martin, J.B., Deuerling, K.M., Collazo, D.F., Marshall, A.T., 2015. Exposure age and climate controls on weathering in deglaciated watersheds of western Greenland. Geochim. Cosmochim. Acta 170, 157–172.

Souchez, R., Lemmens, M., Lorrain, R., Tison, J.-L., Jouzel, J., Sugden, D., 1990. Influence of hydroxyl-bearing minerals on the isotopic composition of ice from the basal zone of an ice sheet. Nature 345, 244–246.

Spence, J., Telmer, K., 2005. The role of sulfur in chemical weathering and atmospheric CO2 fluxes: evidence from major ions, d13CDIC, and d34SSO4 in rivers of the Canadian Cordillera. Geochim. Cosmochim. Acta 69, 5441–5458.

Tranter, M., 2003. Geochemical Weathering in Glacial and Proglacial Environments. In: Drever, J.I. (Ed.), Treatise on Geochemistry. Elsevier Ltd, pp. 189–205.

Tranter, M., Sharp, M.J., Lamb, H.R., Brown, G.H., Hubbard, B.P., Willis, I.C., 2002. Geochemical weathering at the bed of Haut glacier d'Arolla, Switzerland – a new model. Hydrol. Process. 16, 959–993.

van Tatenhove, F.G.M., Olesen, O.B., 1994. Ground temperature and related permafrost characteristics in west Greenland. Permafrost Periglac. Process. 5, 199–215.

Wadham, J.L., Cooper, R.J., Tranter, M., Hodgkins, R., 2001. Enhancement of glacial solute fluxes in the proglacial zone of a polythermal glacier. J. Glaciol. 47, 378– 386.

Ward, J.V., Malard, F., Tockner, K., Uehlinger, U., 1999. Influence of ground water on surface water conditions in a glacial flood plain of the Swiss Alps. Hydrol. Process. 13, 277–293.

White, A.F., Bullen, T.D., Vivit, D.V., Schulz, M.S., Clow, D.W., 1999. The role of

disseminated calcite in the chemical weathering of granitoid rocks. Geochim. Cosmochim. Acta 63, 1939–1953. https://doi.org/10.1016/S0016-037(99)00082-4.

White, A.F., Schulz, M.S., Lowenstern, J.B., Vivit, D.V., Bullen, T.D., 2005. The ubiquitous nature of accessory calcite in granitoid rocks: implications for weathering, solute evolution, and petrogenesis. Geochim. Cosmochim. Acta 69, 1455–1471.

Willemse, N.W., Koster, E.A., Hoogakker, B., van Tatenhove, F.G.M., 2003. A continuous record of Holocene eolian activity in West Greenland. Quaternary Res. 59, 322–334.

Wimpenny, J., Burton, K.W., James, R.H., Gannoun, A., Mokadem, F., Gíslason, S.R., 2011. The behaviour of magnesium and its isotopes during glacial weathering in an ancient shield terrain in West Greenland. Earth Planet. Sci. Lett. 304, 260– 269.

Yde, J.C., Finster, K.W., Raiswell, R., Steffensen, J.P., Heinemeier, J., Olsen, J., Gunnlaugsson, H.P., Nielsen, O.B., 2010. Basal ice microbiology at the margin of the Greenland ice sheet. Ann. Glaciol. 51, 71–79.

Yde, J.C., Knudsen, N.T., Hasholt, B., Mikkelsen, A.B., 2014. Meltwater chemistry and solute export from a Greenland Ice Sheet catchment, Watson River, West Greenland. J. Hydrol. 519, 2165–2179.

Zarnetske, J.P., Gooseff, M.N., Bowden, W.B., Greenwald, M.J., Brosten, T.R., Bradford, J.H., McNamara, J.P., 2008. Influence of morphology and permafrost dynamics on hyporheic exchange in arctic headwater streams under warming climate conditions. Geophys. Res. Lett. 35, 1–5. https://doi.org/10.1029/2007GL032049.